Document downloaded from:

http://hdl.handle.net/10251/74435

This paper must be cited as:

Vilaplana Cerda, RI.; Sans Tresserras, JÁ.; Manjón Herrera, FJ.; Andrada-Chacón, A.; Sánchez-Benitez, J.; Popescu, C.; Gomis, O.... (2016). Structural and electrical study of the topological insulator SnBi2Te4 at high pressures. Journal of Alloys and Compounds. 685:962-970. doi:10.1016/j.jallcom.2016.06.170.

The final publication is available at

http://dx.doi.org/10.1016/j.jallcom.2016.06.170

Copyright Elsevier

Additional Information

Structural and electrical study of the topological insulator $SnBi_2Te_4$ under compression

R. Vilaplana [a,*], J.A. Sans [b], F.J. Manjón [b], A. Andrada-chacón [c], J. Sánchez-Benítez [c], C. Popescu [d], O. Gomis [a], A.L.J. Pereira [b], B. García-Domene [e], P. Rodríguez-Hernández [f], A. Muñoz [f], D. Daisenberger [g] and O. Oeckler [h]

[a] *Centro de Tecnologías Físicas, MALTA Consolider Team, Universitat Politècnica de València, Valencia, Spain*
[b] *Instituto de Diseño para la Fabricación y Producción Automatizada, MALTA Consolider Team, Universitat Politècnica de València, Valencia, Spain*
[c] *Departamento de Química-Física, MALTA Consolider Team, Universidad Complutense de Madrid, Madrid, Spain*
[d] *ALBA-CELLS, Barcelona, Spain*
[e] *Departamento de Física Aplicada-ICMUV, MALTA Consolider Team, Universidad de Valencia, Valencia, Spain*
[f] *Departamento de Física, Instituto de Materiales y Nanotecnología, MALTA Consolider Team, Universidad de La Laguna, Tenerife, Spain*
[g] *Diamond Light Source Ltd, Oxon, England*
[h] *Institut für Mineralogie, Kristallographie und Materialwissenschaft, Universität Leipzig, Germany*

Abstract

We report high-pressure X-ray diffraction and electrical measurements of the topological insulator $SnBi_2Te_4$ at room temperature. The pressure dependence of the structural properties of the most stable phase of $SnBi_2Te_4$ at ambient conditions (trigonal phase) have been experimentally determined and compared with results of our *ab initio* calculations. Furthermore, a comparison of $SnBi_2Te_4$ with the parent compound Bi_2Te_3 shows that the central Te-Sn-Te trilayer, which substitutes the Te layer at the center of the Te-Bi-Te-Bi-Te layers of Bi_2Te_3, plays a minor role in the compression of $SnBi_2Te_4$. Similar to results for Bi_2Te_3, our resistance measurements and electronic band structure simulations of $SnBi_2Te_4$ at high pressure suggest that this compound exhibits a pressure-induced electronic topological transition between 3.5 and 5.0 GPa.

Keywords: high pressure, X-ray diffraction, transport properties, topological insulators, electronic topological transition

PACS number(s): 31.15.A-, 61.05.cp, 62.20.-x, 62.50.-p, 71.15.Mb

*Corresponding author: Departamento de Física Aplicada, Escuela Politécnica Superior de Alcoy, Universitat Politècnica de València, Placeta Ferràndiz i Carbonell 2, 03802 Alcoy (Alicante), Spain. Tel.: +34 96 652 8426; fax: +34 96 652 8485.
E-mail address: rovilap@fis.upv.es (R. Vilaplana)

1. Introduction

Nowadays, Bi_2Te_3 is considered the best thermoelectric material at ambient temperature **[1,2]**. Numerous studies have been devoted to solid solutions of this material and related compounds, like other binary compounds as SnTe **[1,3-9]**, in order to improve its thermoelectric properties. The number of studies of Bi_2Te_3 and related layered semiconductors has dramatically increased in the last years after the prediction and discovery of Bi_2Te_3, Bi_2Se_3, and Sb_2Te_3 as three-dimensional (3D) topological insulators (TIs). This discovery paved the way to search of new TIs in related materials with a view to future application **[10-22]**. In this regard, recent calculations of several ternary layered compounds have shown that $SnBi_2Te_4$ also behaves as a 3D TI **[23-25]**.

Like the parent compound Bi_2Te_3, $SnBi_2Te_4$ crystallizes in a trigonal structure with space group (S.G.) $R\overline{3}m$ (Nº. 166, Z=3), but with 4 atoms at independent positions (Sn at 3*a* Wyckoff sites and Bi, Te_1 and Te_2 at 6*c* Wyckoff sites) **[3,6,26-30]**. The hexagonal unit cell of Bi_2Te_3 contains three quintuple layer (QL) atomic blocks (Te_1–Bi–Te_2–Bi–Te_1), whereas the unit cell of $SnBi_2Te_4$ contains three septuple layer (SL) atomic blocks (idealized sequence: Te_1–Bi–Te_2–Sn–Te_2–Bi–Te_1). A view of the structures of Bi_2Te_3 and $SnBi_2Te_4$ with the hexagonal unit cell and a detail of the QL and SL are shown in **Figs. 1(a) and 1(b)**, respectively. These structure drawings were done with VESTA code **[31]**. As can be observed, the difference between the structure of $SnBi_2Te_4$ and the structure of the binary parent compound Bi_2Te_3 is that the central Te_2 layer of the Bi_2Te_3 is replaced with a Te_2–Sn–Te_2 trilayer in $SnBi_2Te_4$. In both compounds, layers are piled up along [001] and are joined by weak van der Waals forces, while bonds inside the layers (extended in the (001) plane) have predominantly polar covalent character. In $SnBi_2Te_4$, the Sn atom is located at the center of an almost regular Te octahedron, while Bi is near the center of a distorted Te octahedron, like in Bi_2Te_3. Some experimental studies on $SnBi_2Te_4$ suggest that this compound exhibits a certain disorder in its crystalline structure due to mixed Sn/Bi occupancy of cationic sites **[26,28]**. However, other studies suggest that $SnBi_2Te_4$ has ordered SL atomic blocks **[27,30]**.

To further understand the properties of this interesting compound, we report an experimental study of the structural and electrical properties of the most stable phase of

74 $SnBi_2Te_4$ at ambient conditions by means of synchrotron-based X-ray diffraction (XRD)
75 and electrical resistance measurements at high pressures (HP) up to 9 GPa. Additionally,
76 *ab initio* simulations of structural parameters in ordered $SnBi_2Te_4$ at different pressures
77 have been performed in order to compare them with experimental measurements. The
78 main objective of this study is to characterize the structure of the low pressure phase of
79 this compound under compression (with the aim to compare it with the behavior of its
80 parent compound Bi_2Te_3) and to study the possible existence of a pressure-induced
81 electronic topological transition (ETT) in $SnBi_2Te_4$, as it occurs in Bi_2Te_3 and related
82 compounds **[32-43]**. For this last purpose, we have carried out resistance measurements
83 and theoretical electronic band structure simulations in $SnBi_2Te_4$ at different pressures,
84 which have been analyzed in comparison to its parent compound Bi_2Te_3.
85

86 **2. Experimental section**

87 *2.1. Sample preparation and characterization*

88 Bulk samples of $SnBi_2Te_4$ were prepared by melting stoichiometric amounts of the pure
89 elements Sn (99.999%, Smart Elements), Bi (99.999%, Smart Elements) and Te
90 (99.999%, Alfa Aesar) at 890 ºC for 4h in sealed silica glass ampoules under argon
91 atmosphere and subsequent annealing at 500 ºC for 160h, similarly to those of $SnSb_2Te_4$
92 **[44]**. Representative parts of the samples were crushed to powders and fixed on Mylar
93 foils with hair-fixing spray to collect powder diffraction patterns on a Huber G670 powder
94 diffractometer equipped with an image plate detector (Cu-$K_{\alpha1}$ radiation, Ge(111)
95 monochromator, λ= 1.54051 Å) in Guinier geometry. Rietveld refinement confirmed the
96 high purity of the synthesized sample.
97

98 *2.2. Measurements*

99 Two powder angle-dispersive HP-XRD experiments at ambient temperature were carried
100 out. The first one up to 37.2 GPa was conducted at beamline I15 of Diamond Light Source
101 using a monochromatic X-ray beam (λ= 0.42408 Å). $SnBi_2Te_4$ powder and a strip of Cu
102 were loaded in a 150-μm diameter hole of an Inconel gasket inside a membrane-type
103 diamond-anvil cell (DAC) with diamond-culet sizes of 350 μm. He gas was used as
104 pressure-transmitting medium. The X-ray beam was focused down to 70 x 70 μm^2 using
105 Kickpatrick-Baez mirrors. A pinhole assembly placed before the sample position was
106 used to collimate the beam down to 30 μm (round diameter) and as a clean-up aperture

107 for filtering out the tail of the X-ray beam. Images were collected using a MAR345 image
108 plate located at 430 mm from the sample. In order to obtain more data points of the low-
109 pressure phase, a second HP-XRD experiment was conducted at beamline MSPD-BL04
110 **[45]** of ALBA Synchrotron Light Source using monochromatic radiation (λ= 0.4246 Å)
111 up to 8 GPa. Silicon oil was used as a pressure-transmitting medium in this second
112 experiment. In both experiments, pressure was determined using the copper equation of
113 state (EOS) with parameters obtained by a Vinet equation **[46]**. Diffraction patterns were
114 integrated as a function of 2θ using FIT2D in order to give conventional, one-dimensional
115 diffraction profiles **[47].** Indexing and Le Bail refinement in the powder diffraction
116 patterns was performed using UNITCELL **[48]**, POWDERCELL **[49]** and GSAS **[50,51]**
117 program packages. Although the monochromatic radiation of both beamlines corresponds
118 to Sn K-edge absorption, Rietveld refinements taking into account resonant X-ray
119 diffraction were not successful due to pronounced preferred orientation. Consequently,
120 we have performed Le Bail fitting which allows refining unit cell parameters but not
121 atomic positions.

122 Electrical resistance measurements at HP were performed by using the standard four-
123 point probe van der Pauw method **[52]** in a modified Merrill-Bassett-type DAC with 400
124 μm culet diamonds. Thin flakes approximately 30 μm thick and with a 100 x 100 μm^2
125 surface for the measurements were obtained from cleaving the original single crystals. As
126 the accurate measurement of the sample dimensions (thickness and the distance between
127 the four electrodes inside the DAC) was impossible, the resistivity could not be
128 calculated. The electrical resistance was measured using four 20μm-thick copper-
129 beryllium wires in two different arrangements: in the first one, samples were placed
130 directly between the anvils without any pressure transmitting medium; i.e., under uniaxial
131 conditions. In the second one, measurements were performed under quasi-hydrostatic
132 conditions by using stainless steel gaskets and CsI powder as a pressure transmitting
133 medium. In both arrangements the luminescence of ruby powder was used to determine
134 pressure **[53,54]**. In both setups, measurements were conducted up to 10 GPa and the R_1
135 and R_2 ruby lines remained well resolved to obtain accurately the pressure in the whole
136 pressure range. In the two experiments, the electrical resistance showed similar trends,
137 probably due to the anisotropic (layered) and soft nature of the crystals.

138

139 **3. Theoretical calculations**

140 *Ab initio* total-energy calculations were carried out for $SnBi_2Te_4$ in the low-pressure
141 trigonal $R\overline{3}m$ structure without considering disorder. They were performed within the
142 density functional theory (DFT) **[55]** using the plane-wave method and the
143 pseudopotential theory with the Vienna Ab initio Simulation Package (VASP) **[56,57]**.
144 The projector-augmented wave scheme (PAW) **[58]** was used as implemented in this
145 package and the basis set of plane waves extended up to an energy cutoff of 320 eV to
146 achieve highly converged results and accurate description of the electronic properties. Bi
147 semicore *d* orbitals were included within a scalar relativistic scheme to take into account
148 the spin-orbit interaction (SOI). The exchange-correlation energy was described in the
149 generalized gradient approximation (GGA) with the PBEsol **[59]** prescription. In order to
150 obtain very well converged energies and forces, a 6x6x6 grid of special k-points was
151 employed for the integration over the Brillouin zone (BZ). At selected volumes, the
152 structures were fully relaxed to their optimized configuration through the calculation of
153 the forces on atoms and the stress tensor. In the optimized configurations, the forces on
154 the atoms were less than 0.002 eV/Å and the deviations of the stress tensor from a
155 diagonal hydrostatic form are smaller than 1 kbar (0.1 GPa). The electronic band
156 structures along high symmetry directions and the corresponding density of states (DOS)
157 were calculated with a mesh of 18x18x18 k-points.

158 **4. Results and Discussion**

159 As mentioned previously, $SnBi_2Te_4$ is a layered structure composed of SL atomic blocks
160 piled along the hexagonal *c* axis and joined by weak van der Waals forces. The XRD
161 pattern of $SnBi_2Te_4$ at ambient conditions is shown in **Figure 2**. Le Bail refinement
162 yielded the following hexagonal lattice parameters at ambient pressure: a = 4.40283(10)
163 Å, c = 41.7139(22) Å, resulting in a volume of V_0 = 700.28(6) Å^3. Rietveld refinement of
164 resonant XRD data in comparable as-grown samples of $SnSb_2Te_4$ revealed the presence
165 of some cation disorder **[44]**, which is also expected in $SnBi_2Te_4$. However, since Rietveld
166 refinement proved impossible in this work, we cannot discuss the evolution of disorder
167 with pressure in $SnBi_2Te_4$. In this respect, it must be noted that the lattice parameters
168 obtained by Le Bail refinement show good agreement with our theoretical ones that do
169 not consider disorder (see **Table I**) and with experimental ones previously reported
170 **[3,6,8,25,26,28,29]**. Furthermore, our theoretical values also compare well to previously
171 reported calculations **[25]**. For the sake of completeness, our theoretical fractional atomic

172 coordinates for the trigonal phase of $SnBi_2Te_4$ at ambient conditions are reported in **Table**
173 **II**.
174
175 **Figure 3** shows powder HP-XRD patterns of $SnBi_2Te_4$ at selected pressures up to 7.9
176 GPa. New reflections (see asterisks in **Fig. 3**) appear at 7 GPa and increase at higher
177 pressure, thus indicating a phase transition that is reversible after decreasing pressure
178 from 8 GPa (see pattern of the recovered sample at 2.4 GPa on top of **Fig. 3**). We want to
179 comment that the discussion of the structure of the high-pressure phase of $SnBi_2Te_4$ above
180 7 GPa is out of the scope of the present work and will be reported elsewhere.

181 The pressure dependence of the unit cell volume of $SnBi_2Te_4$ is shown in **Fig. 4**. Full and
182 open red circles represent the measurements carried out in the first and the second
183 experiment, respectively. The bulk modulus of $SnBi_2Te_4$ has been characterized using a
184 third-order Birch-Murnaghan equation of state (BM-EOS) **[60]. Table III** shows the
185 experimental and theoretical values of the unit cell volume, bulk modulus and its pressure
186 derivative at ambient pressure for $SnBi_2Te_4$. Values for Bi_2Te_3 have also been added for
187 comparison. Experimental values for $SnBi_2Te_4$ are in good agreement with theoretical
188 calculations and the bulk modulus has a similar value in both $SnBi_2Te_4$ and Bi_2Te_3. This
189 result suggests that the Sn octahedrons in the center of the SLs do not play an important
190 role in the resistance of $SnBi_2Te_4$ to compression at low pressures. Moreover, this result
191 is consistent with what is expected for the layered structure of both compounds since the
192 large compressibility of both semiconductors at room pressure is determined by the weak
193 van der Waals forces between multiple adjacent layers piled up along the *c* axis.

194 The evolution of the lattice parameters under pressure is displayed in **Fig. 5**. In order to
195 obtain the experimental and theoretical axial compressibilities of the *a* and *c* axes, we
196 have fitted the lattice parameters obtained by Le Bail fitting and by *ab initio* calculations
197 to a modified Murnaghan EOS **[64]**. The axial bulk modulus B_{0i} obtained for each lattice
198 parameter *i* allows us to determine the axial compressibility as $\kappa_i = \frac{1}{3B_{0i}}$. **Table IV** shows
199 the experimental and theoretical results of the a and caxial bulk moduli and
200 compressibilities in $SnBi_2Te_4$ and their comparison to Bi_2Te_3. The axial compressibility
201 of the *c* axis is almost twice that of the *a* axis in $SnBi_2Te_4$. The same result is observed in
202 Bi_2Te_3. Furthermore, the axial bulk moduli are similar, but slightly larger, in $SnBi_2Te_4$

203 than in Bi_2Te_3. Since the different bulk moduli fall within the experimental and theoretical
204 uncertainties, it is difficult to ascertain whether this result is due to the substitution of the
205 central Te layer in Bi_2Te_3 by the Te-Sn-Te layer in $SnBi_2Te_4$. Finally, it is worth to
206 mention that a minimum occurs between 3 and 4 GPa in the *c/a* ratio of our experimental
207 and theoretical data for $SnBi_2Te_4$ (see inset in **Fig. 5**), as it was previously reported for
208 Bi_2Te_3 **[40,41]**.
209
210 In order to better understand the structural behavior of $SnBi_2Te_4$ under compression we
211 have plotted in **Fig. 6** the pressure dependence of the theoretical interlayer Te_1-Te_1
212 distance along the c-axis and intralayer Te_1-Bi, Te_2-Bi and Te_2-Sn distances inside the
213 SL. These distances show the pressure evolution of the irregular Bi and quasi-regular Sn
214 octahedra, respectively. It can be clearly observed that the quasi-regular Sn octahedron
215 (note that all Sn-Te distances are equal but the Te-Sn-Te angles are slightly different from
216 90º) is slightly compressed as indicated by the decrease of the Te_2-Sn distance. On the
217 other hand, the distorted Bi octahedron is not so much compressed (Te_2-Bi distance
218 decreases while Te_1-Bi bond distance increases) and tends to become more regular on
219 increasing pressure. In any case, most of the compression of the trigonal phase at low
220 pressure is clearly related to the strong decrease of the Te_1-Te_1 interlayer distance with
221 pressure, especially below 4 GPa. The change in the slope of the interlayer distance above
222 4 GPa is related to the strengthening of van der Waals interactions at high pressure as
223 observed in many layered and molecular compounds **[65,66]**. **Fig. 6** also shows the
224 pressure dependence of the theoretical interlayer Te_1-Te_1 distance along [001] and
225 intralayer Te_1-Bi, and Te_2-Bi distances inside the QL of the parent compound Bi_2Te_3
226 taken from a previous calculation **[37]**. It can be observed that our calculations indicate
227 that the Bi octahedron is slightly more compressed in $SnBi_2Te_4$ than in Bi_2Te_3. (Te_2-Bi
228 starts at the same but has steeper slope and ends at a smaller value and Te_1-Bi seems
229 parallel between the two compounds). Therefore, the structural differences between both
230 compounds under compression are mainly related to the Sn octahedron and to a lesser
231 extent to the Bi octahedron.
232
233 All the above mentioned results suggest that it is likely that $SnBi_2Te_4$ shows a pressure-
234 induced ETT before undergoing a structural phase transition, just like it occurs in Bi_2Te_3
235 around 3-4 GPa **[32,34,35,37,40-43].** The ETT is an isostructural transition of $2^{1/2}$ order

236 which shows no volume discontinuity, where the Wyckoff positions of atoms are not
237 modified during the transition. Since there is neither associated volume collapse during
238 the transition nor change of the symmetry of the atomic positions, it is difficult to detect
239 by XRD measurements. The ETT is a consequence of a topological change in the Fermi
240 surface related to the passage of an extremum of the electron energy band (equivalent to
241 the van Hove peak in the density of states) through the Fermi level. Apart from the direct
242 observation of the changes at the Fermi surface by means of angle-resolved photoelectron
243 spectroscopy, transport measurements have also been used as one of the most convincing
244 ways to detect ETTs **[32,34,35,43]**. However, other transport properties such as electrical
245 and thermal resistances, and the thermal expansion coefficient, could also provide subtle
246 evidences for ETTs, as discussed by Kechin *et al.* **[67]** for Zn. In this regard, we have
247 carried out resistance measurements complemented with electronic band structure
248 calculations in order to shed some light into the possible pressure-driven ETT in
249 $SnBi_2Te_4$.
250
251 **Figure 7** shows the resistance of $SnBi_2Te_4$ as measured during loading and unloading
252 process up to and from 9.0 GPa (with CsI as pressure-transmitting medium). As can be
253 observed, an increase of the resistance occurs between 3.5 and 5.0 GPa, not far from the
254 minimum in the *c/a* ratio of our experimental and theoretical data for $SnBi_2Te_4$. Note that
255 an increase in resistance was also observed previously in other ETT studies **[68]**. This
256 result suggests that in $SnBi_2Te_4$, a pressure-induced ETT could occur during this pressure
257 interval, similar to the parent compound Bi_2Te_3 where changes around 3-4 GPa were
258 observed before the first-order phase transition above 8.0 GPa **[32,34,35,37,40-43]**. On
259 the other hand, a decrease of the resistance with pressure takes place between 7-8 GPa,
260 which must be related to the high pressure phase evidenced by XRD measurements above
261 7 GPa. Finally, we have to note that the resistance recovers with some hysteresis when
262 pressure is released, thus indicating that the phase transition above 7 GPa in $SnBi_2Te_4$ is
263 reversible, as it was also recently observed in Bi_2Te_3 **[69]**.
264
265 In order support the observation of a possible pressure-induced ETT in $SnBi_2Te_4$, we have
266 performed electronic band structure calculations at different pressures (see **Fig. 8**) and
267 have compared them with those of Bi_2Te_3 **[37]** (see **Fig. 9**). The calculations show that
268 $SnBi_2Te_4$ is an indirect semiconductor at 1 GPa (with a narrow energy bandgap around

269 0.1 eV) which has the valence band maximum (VBM) along the L-Z direction (V_1) and
270 the conduction band minimum (CBM) along the Γ-Z direction (C_1). Close in energy to
271 these extrema, our calculations show a second VBM along the Z-F direction (V_2) and a
272 second CBM along the F-Γ direction (C_2).

273 According to recent transport measurements at ambient conditions, $SnBi_2Te_4$ is prone to
274 be an extrinsic p-type semiconductor with up to 10^{20} holes/cm^3 due to off-stoichiometry
275 defects **[70]**. In our calculations for a pure intrinsic semiconductor, the VBM is taken as
276 a reference energy (0 eV), so in a highly-doped semiconductor, the Fermi level must be
277 well inside the valence band as shown in **Fig. 8** by the dashed red line. At zero pressure,
278 it can be thought that the Fermi level is located between V_1 and V_2. However, as pressure
279 increases, the difference in energy between V_1 and V_2 decreases so the Fermi level can
280 cross V_2 (see **Fig. 8** at 3.9 GPa) and cause a pressure-induced ETT in $SnBi_2Te_4$, which
281 would explain the change observed in resistance above 3.5 GPa.

282 In a recent study of Bi_2Te_3, a similar reasoning was used to explain the observed pressure-
283 induced ETT **[42]**. Calculations of our previous study of Bi_2Te_3 are in agreement with
284 this recent work. **Fig. 9** shows our calculated electronic band structure of Bi_2Te_3 at
285 different pressures. In good agreement with the recent calculations **[42]**, two VBMs (V_1
286 and V_2) very close in energy are observed at 1 zero pressure along the L-Z and Z-F
287 directions; however, as pressure increases both VBM tend to separate in energy.
288 Therefore, taking into account that Bi_2Te_3 is also a p-type semiconductor it is conceivable
289 that both VBM are above the Fermi level (red dashed line in **Fig. 9**) at low pressures;
290 however, it is expected that the V_2 VBM cross below the Fermi level at high pressures,
291 between 2 and 4 GPa depending on the hole concentration. This fact is responsible for the
292 pressure-induced ETT observed in Bi_2Te_3. These theoretical results on Bi_2Te_3 give us
293 confidence about our present calculations for $SnBi_2Te_4$.

294

295 In summary, our theoretical simulations of $SnBi_2Te_4$ give support to a possible pressure-
296 induced ETT between 3.5 and 5 GPa, which occurs prior to the first order phase transition
297 taking place. This pressure range for the ETT is consistent with the pressure at which we
298 observed an increase of resistance.

299

300 **5. Concluding remarks**

301
302 We have investigated the structural and electric properties of the trigonal phase of
303 $SnBi_2Te_4$ as a function of pressure. A reversible phase transition is observed above 7.0
304 GPa in $SnBi_2Te_4$, as it was also observed in Bi_2Te_3. The bulk equation of state and the
305 axial compressibilities at zero pressure of the low-pressure phase of $SnBi_2Te_4$ have been
306 determined. By comparison with Bi_2Te_3, our data confirm that the presence of an
307 additional central Te-Sn-Te layer in $SnBi_2Te_4$ induces subtle differences in the pressure
308 dependence of the structural parameters, but not on the transition pressure to the high-
309 pressure phase in both compounds. Similar volume and axial bulk moduli have been
310 obtained for both compounds and a minimum in the *c/a* ratio (around 3.5 GPa) is observed
311 in $SnBi_2Te_4$, similar to that observed in Bi_2Te_3. Consequently, the Sn octahedron at the
312 center of the layer seems to play a minor role in the compression of the low-pressure
313 phase of $SnBi_2Te_4$ under quasi-hydrostatic conditions. Finally, our high-pressure
314 resistance measurements in $SnBi_2Te_4$ show an increase of resistance between 3.5 and 5.0
315 GPa not far from pressure where the minimum in the c/a ratio occurs. These results
316 suggest the existence of a pressure-induced ETT in $SnBi_2Te_4$ similar to what occurs in
317 Bi_2Te_3 around 3-4 GPa. In this regard, additional high-pressure measurements, including
318 Raman scattering and magneto-transport measurements, as well as additional calculations
319 are underway in order to study in detail the presence of a pressure-induced ETT in
320 $SnBi_2Te_4$.
321
322 **Acknowledgments**
323
324 We thank Dr. Philipp Urban for preparing the sample. This work has been performed
325 under financial support from Spanish MINECO under projects MAT2013-46649-C4-2-
326 P, MAT2015-71070-REDC and CTQ2015-67755-C2-1-R and from Spanish Ministerio
327 de Educación, Cultura y Deporte as part of "Programa Campus de Excelencia
328 Internacional/Programa de Valoración y Recursos Conjuntos de I+D+i VLC/CAMPUS"
329 through projects SP20140701 and SP20140871. One of the experiments were performed
330 at MSPD-BL04 beamline at ALBA Synchrotron with the collaboration of ALBA staff.
331 J.A.S. thanks "Juan de la Cierva" fellowship program for funding. A.A.-C. and J.S.-B.
332 are also grateful to Spanish MINECO for the FPI (BES-2013-066112) and Ramón y Cajal
333 (RyC-2010-06276) fellowships. We acknowledge Diamond Light Source for time on
334 beamline I15 under Proposal EE9102.

335

336 **References**

337 [1] D. M. Rowe, CRC Handbook of Thermoelectrics, (CRC Press Inc., New York,
338 1995).
339 [2] R. Venkatasubramanian, E. Siivola, T. Colpitts, and B. O'Quinn, Nature **413**, 597
340 (2001).
341 [3] L.A. Kuznetsova, V.L. Kuznetsov and D.M. Rowe, J. Phys. Chem. Solids, **61**, 1269
342 (2000).
343 [4] X.-S. Zhou, Y. Deng, C.-W. Nan, and Y.-H. Lin, J. Alloys Comp. **352**, 328 (2003).
344 [5] X.-S. Zhou, Y. Deng, G.D. Wei, J. Liu, and C.-W. Nan, Sci. China **46**, 509 (2003).
345 [6] L.E. Shelimova, O.G. Karpinskii, P.P. Konstantinov, E.S. Avilov, M.A. Kretova,
346 V.S. Zemskov, Inorg. Mat. **40**, 451 (2004).
347 [7] G. J. Snyder and E. S. Toberer, Nat. Mater. **7**, 105 (2008).
348 [8] B.A. Kuropatwa and H. Kleinke, Z. Anorg. Allg. Chem. **638**, 2640 (2012).
349 [9] L. Pan et al., J. Solid State Chem. **225**, 168 (2015).
350 [10] L. Fu and C. L. Kane, *Phys. Rev. B* **76**, 045302 (2007).
351 [11] L. Fu, C.L. Kane and E.J. Mele, *Phys. Rev. Lett.* **98**, 106803 (2007).
352 [12] J. C. Y. Teo, L. Fu, and C. L. Kane, *Phys. Rev. B* **78**, 045426 (2008).
353 [13] X.-L. Qi, T. L. Hughes, and S. C. Zhang, *Phys. Rev. B* **78**,195424 (2008).
354 [14] Y. Xia, D. Qian, D. Hsieh, L. Wray, A. Pal, H. Lin, A. Bansil, D. Grauer, Y. S.
355 Hor, R. J. Cava, and M.Z. Hasan, *Nat. Phys.* **5**, 398 (2009).
356 [15] H. Zhang, C.X. Liu, X.L. Qi, X. Dai, Z. Fang and S.C. Zhang, *Nat. Phys.* **5,** 438
357 (2009).
358 [16] Y. L. Chen, J. G. Analytis, J. H. Chu, Z. K. Liu, S. K. Mo, X. L. Qi, H. J. Zhang, D.
359 H. Lu, X. Dai, Z. Fang, S. C. Zhang, I. R. Fisher, Z. Hussain, and Z. X. Shen, Science
360 **325**, 178 (2009).
361 [17] D. Hsieh et al., *Phys. Rev. Lett.* **103**, 146401 (2009).
362 [18] J.E. Moore, *Nature* **464**, 194 (2010).
363 [19] M.Z. Hasan and C.L. Kane, Rev. Mod. Phys. **82**, 3045 (2010).
364 [20] L. Fu, *Phys. Rev. Lett.* **106,** 106802 (2011).
365 [21] T.V. Menshchikova, S.V. Eremeev, E.V. Chulkov, JETP Letters **94**, 106 (2011).
366 [22] S. V. Eremeev, G. Landolt, T. V. Menshchikova, B. Slomski,Y. M. Koroteev, Z. S.
367 Aliev, M. B. Babanly, J. Henk, A. Ernst, L. Patthey, A. Eich, A. A. Khajetoorians, J.
368 Hagemeister, O. Pietzsch, J. Wiebe, R. Wiesendanger, P. M. Echenique, S. S. Tsirkin, I.
369 R. Amiraslanov, J. H. Dil and E. V. Chulkov, *Nature Commun.* **3**, 635 (2012).
370 [23] T.V. Menshchikova, et al., *Appl. Surf. Sci.* 267, 1 (2013).
371 [24] S.V. Eremeev,T.V. Menshchikova, I.V. Silkin, M.G. Vergniory, P.M. Echenique,
372 and E. V. Chulkov; *Phys. Rev. B* **91**, 245145 (2015).
373 [25] M.G. Vergniory, T.V. Menshchikova, I.V. Silkin, Yu.M. Koroteev, S.V. Eremeev,
374 and E.V. Chulkov, *Phys. Rev. B* **92**, 045134 (2015)
375 [26] T.B. Zhukova, and A.I. Zaslavskii, *Sov. Phys. Crystallogr.* **16**, 796 (1971).
376 [27] F. Casula, L. Deiana and A. Podda, J. Phys.: Condens. Matter 3, 1461 (1991).
377 [28] K. Adouby, A.A. Toure, G. Kra, et al. *C. R. Acad. Sci., Chem.* **3,** 51 (2000).

378 [29] O.G. Karpinskii, L.E. Shelimova, M.A. Kretova, E.S. Avilov, and V.S. Zemskov,
379 Inorg. Mat. 39, 240 (2003).
380 [30] F. Ledda, C. Muntoni, S. Serci, and L. Pellerito, *Chem. Phys. Lett.* **134**, 545 (1987).
381 [31] K. Momma and F. Izumi, *J. Appl. Crystallogr.* **44** (2011).
382 [32] E.S. Itskevitch, L.M. Kashirskaya, and V.F. Kraidenov, Semicond. 31, 276 (1997).
383 [33] D. A. Polvani, J. F. Meng, N. V. Chandra Shekar, J. Sharp, and J. V. Badding,
384 Chem. Mater. 13, 2068 (2001).
385 [34] S. V. Ovsyannikov, V. V. Shchennikov, G. V. Vorontsov, A. Y. Manakov, A.Y
386 Likhacheva, and V. A. Kulbachinskii, J. Appl. Phys. **104**, 053713 (2008)
387 [35] M.K. Jacobsen, R.S. Kumar, A.L. Cornelius, S.V. Sinogeiken, and M.F. Nicol, *AIP*
388 *Conf. Proc.* **955**, 171 (2007).
389 [36] R. Vilaplana, D. Santamaría-Pérez, O. Gomis, F. J. Manjón, J. González, A. Segura,
390 A. Muñoz, P. Rodríguez-Hernández, E. Pérez-González, V. Marín-Borrás, V. Muñoz-
391 Sanjose, C. Drasar, and V. Kucek, *Phys. Rev. B* **84**, 184110 (2011).
392 [37] R. Vilaplana, O. Gomis, F. J. Manjón, A. Segura, E. Perez-González, P. Rodríguez-
393 Hernández, A. Muñoz, J. González, V. Marín-Borras, V. Muñoz-Sanjosé, C. Drasar,
394 Kucek, *Phys. Rev. B.* **84,** 104112 (2011).
395 [38] O. Gomis, R. Vilaplana, F. J. Manjón, P. Rodríguez-Hernández, E. Pérez-González,
396 A. Muñoz, V. Kucek, and C. Drasar, *Phys. Rev. B* **84**, 174305 (2011).
397 [39] F.J. Manjón, R. Vilaplana, O. Gomis, E. Pérez-González, D. Santamaría-Pérez, V.
398 Marín-Borrás, A. Segura, J. González, P. Rodríguez-Hernández, A.Muñoz, C. Drasar,
399 V. Kucek, and V. Muñoz-Sanjosé, Physica Status Solidi (b) **250**, 669 (2013).
400 [40] A. Nakayama, M. Einaga, Y. Tanabe, S. Nakano, F. Ishikawa and Y. Yamada, *High*
401 *Pressure Res.* **29,** 245 (2009)
402 [41] A. Polian, M. Gauthier, S.M. Souza, D.M. Triches, J. Cardoso de Lima and T. A.
403 Grandi, *Phys. Rev. B* **83,** 113106 (2011).
404 [42] W. Ibarra-Hernández, M. J. Verstraete and J.Y. Raty, *Phys. Rev. B* **90** 245204 (2014).
405 [43] J. Zhang, C. Liu, X. Zhang, F. Ke, Y. Han,G. Peng,Y. Ma, and C. Gao, *Appl. Phys.*
406 *Lett.* **103**, 052102 (2013).
407 [44] O. Oeckler, M. N. Schneider, F. Fahrnbauer, and G.Vaughan, *Solid State Sci.* **13**,
408 1157 (2011).
409 [45] F. Fauth, I. Peral, C. Popescu and M. Knapp, The New Material Science Powder
410 Diffraction Beamline at ALBA Synchrotron. Powder Diffr. **28,** 360 (2013).
411 [46] A. Dewaele, P. Loubeyre, and M. Mezouar, *Phys. Rev. B* **70**, 094112 (2004).
412 [47] A. P. Hammersley, S. O. Svensson, M. Hanfland, A. N. Fitch, and D. Häusermann,
413 *High Pressure Res.*, **14,** 235 (1996).
414 [48] T. J. B. Holland, and S. A. T. Redfern, *Miner. Mag.*, **61**, 65 (1997).
415 [49] W. Kraus, and G. Nolze, *J. Appl. Crystallogr.* **29,** 301 (1996).
416 [50] A. C. Larson, and R. B. von Dreele, *LANL Report* **86**,748, (2004).
417 [51] B. H. Toby, *J. Appl. Crystallogr.* **34**, 210 (2001).
418 [52] van der Paw J. L. Philips Res. Rep. **13**, 1 (1958).
419 [53] H. K. Mao, J. Xu, and P. M. Bell, *J. Geophys. Res.* **91**, 4673 (1986).
420 [54] K. Syassen, *High Press. Res.* **28**, 75 (2008).
421 [55] P. Hohenberg, W. Kohn, *Phys. Rev.* **136,** 3864 (1964).

[56] G. Kresse, J. Hafner, *Phys. Rev. B* **47** 558 (1993).
[57] G. Kresse, J. Furthmüller, *Phys. Rev. B* **54,** 11169 (1996).
[58] P.E. Blöchl, *Phys. Rev. B* **50**, 17953 (1994).
[59] J.P. Perdew, A. Ruzsinszky, G.I. Csonka, O.A. Vydrow, G.E. Suseria, L.A. Constantin, X. Zhou and K. Burke, *Phys. Rev. Lett.* **100**, 136406 (2008).
[60] F. Birch, J. Appl. Phys. 9 (1938) 279.
[61] L. Zhu, H. Wang, Y. Wang, J. Lv, Y. Ma, Q. Cui, Y. Ma, and G. Zou, *Phys. Rev. Lett.* **106,** 145501 (2011).
[62] M. Einaga, A. Ohmura, A. Nakayama, F. Ishikawa, Y. Yamada and S. Nakano, *Phys. Rev. B* **83,** (2011) 092102.
[63] S. Feng, S.M. Li and H.Z. Fu, *Comp. Mat. Sci.* **82,** 45 (2014).
[64] M. D. Frogley, J. L. Sly and D. J. Dunstan, *Phys. Rev. B* **58**, 12579 (1998).
[65] J.A. Sans, F.J. Manjón, A.L.J. Pereira, R. Vilaplana, O. Gomis, A. Segura, A. Muñoz, P. Rodríguez-Hernández, C. Popescu, C. Drasar, and P. Ruleova, Phys. Rev. B 93, 024110 (2016).
[66] J.A. Sans, F.J. Manjón, C. Popescu, V.P. Cuencia-Gotor, O. Gomis, A. Muñoz, P. Rodríguez-Hernández, J. Contreras-García, J. Pellicer-Porres, A.L.J. Pereira, D. Santamaría-Pérez, and A. Segura, Phys. Rev. B 93, 054102 (2016).
[67] V.V. Kechin, *Phys. Rev. B* **63** 045119 (2001).
[68] A. B. Garg, V. Vijayakumar, P. Modak, D. M. Gaitonde, R. S. Rao, B. K.Godwal and S.K. Sikka, *J. Phys.: Condens. Matter* **14,** 8795 (2002).
[69] G. Xiao, K. Wang, L. Zhu, X. Tan, Y.C. Qiao, K. Yang, Y.M. Ma, B.B. Liu, W.T. Zheng, and B. Zou, *J. Phys. Chem C* **119,** 3843 (2015).
[70] L. Pan, J. Li, D. Berardan, and N. Dragoe, *J. Solid State Chem.* **225**, 168 (2015).

Table I. Experimental (Exp) and theoretical (The) lattice parameters and volume corresponding to the trigonal phase of $SnBi_2Te_4$ at ambient conditions.

a (Å)	**c (Å)**	**V_0(Å^3)**	**Ref.**

4.40283(10)	41.7139(22)	700.286	Exp[a]
4.411	41.511	699.468	Exp[b]
4.3954(4)	41.606(1)	696.119	Exp[c]
4.404(1)	41.612(5)	698.946	Exp[d]
4.405(1)	41.60(1)	699.062	Exp[e]
4.40387(3)	41.6003(4)	698.708	Exp[f]
4.3915	41.1948	688.016	The[a*]
4.39	41.61	694.476	The[g*]

459 This work[a], Ref. [26][b], Ref. [28][c], Ref.[3][d], Refs. [29] and [6][e], Ref. [8][f], Ref [25][g]

460 *All calculations include SOI.

461

462

463

464

465 **Table II.** Theoretical atomic positions corresponding to the trigonal phase of $SnBi_2Te_4$ at

466 zero pressure.

Atoms	**Sites**	**x**	**y**	**z**
Sn	3a	0	0	0
Bi	6c	0	0	0.4268
Te_1	6c	0	0	0.1349
Te_2	6c	0	0	0.2890

467

468

469

470

471

472

473

474 **Table III.** Experimental (Exp) and theoretical (The) parameters of the third-order BM-

475 EOS of $SnBi_2Te_4$ and Bi_2Te_3 at ambient conditions: volume (V_0), bulk modulus (B_0), and its

476 pressure derivative (B_0').

Compound	V_0 (Å^3)	B_0 (GPa)	B_0’	Character
$SnBi_2Te_4$	697.8(1)	35(2)	6.2(7)	Exp[a]
	688.0(5)	41.1(9)	5.8(3)	The[a]
Bi_2Te_3	507.6	56.2	2.1	Exp[b]
		21.9*	17.1	Exp[c]
		38.2†	4.6	
	505.1	35.1‡	6.2	Exp[d]
	510.4	46.3	3.6	Exp[e]
		50.1	3.0	
		32.5	10.1	Exp[f]
	500.0	41.6	4.68	The[g]
		28.1		The[h]
		40.3		The[i]

[a] This work, [b] Ref. 35, [c] Ref. 40, [d] Ref. 41, [e] Ref. 61, [f] Ref. 62, [g] Ref. 37, [h] Ref. 42, [i] Ref. 63.
* Below 2 GPa, † above 2 GPa, ‡ whole pressure range

Table IV. Experimental (Exp) and theoretical (The) and bulk moduli (B_0) of the lattice parameters of $SnBi_2Te_4$ and their associated axial compressibilities associated. Same information for Bi_2Te_3 is provided for comparison.

Material	B_{0a} (GPa)	B_{0c} (GPa)	κ_a (10^{-3} GPa^{-1})	κ_c (10^{-3} GPa^{-1})	Ref.
$SnBi_2Te_4$	42.3(1.7)	25.3(1.7)	7.9(3)	13.1(9)	Exp.[a]
	48.0(1.4)	30(2)	6.9(7)	11.1(7)	The (GGA-PBEsol)[a]
Bi_2Te_3	39.9(1.5)	21.9(1.2)	8.4(3)	15.2(8)	Exp.[b]
	46.1(6)	29(3)	7.2(1)	11.6(1.2)	The (GGA-PBEsol)[c]

[a] This work. Calculations including SOI.
[b] Ref. 41
[c] Ref. 37

Figure captions

Figure 1. (Color online)
(a) Bi_2Te_3 unit cell at ambient pressure with one QL highlighted. (b) SnB_2Te_4 unit cell at ambient pressure with one SL highlighted. Blue, magenta and brown colors correspond to Sn, Bi and Te atoms, respectively.

Figure 2. (Color online)

499 Powder XRD pattern of $SnBi_2Te_4$ at ambient pressure (open symbols). Le Bail refinement
500 (solid red line) and residuals are also plotted. Tick marks correspond to $SnBi_2Te_4$
501 reflections of the trigonal phase.
502
503 **Figure 3. (Color online)**
504 Powder XRD patterns of $SnBi_2Te_4$ at selected pressures up to 7.9 GPa. Patterns shifted
505 along vertical axis for comparison. Asterisks indicate reflections of the new phase and the
506 plus symbol represents the (111) copper Bragg reflection. The pattern of $SnBi_2Te_4$ at 2.4
507 GPa on decreasing pressure is shown at the top.

508 **Figure 4. (Color online)** Experimental (symbols) and theoretical (solid lines) pressure
509 dependence of the unit-cell volume of $SnBi_2Te_4$ under compression. Experimental data
510 are fit to a third-order BM-EOS (dashed lines). Full and open circles represent the
511 measurements carried out at Diamond and Alba synchrotron facilities, respectively.

512 **Figure 5. (Color online)** Experimental (symbols) and (solid lines) pressure dependence
513 of the lattice parameters of $SnBi_2Te_4$ under compression. Full and open circles represent
514 the measurements carried out at Diamond and Alba synchrotron facilities, respectively.
515 Inset shows the experimental (symbols) and theoretical (dashed line) pressure dependence
516 of the axial c/a ratio. Solid red line represents the fit of experimental data.

517 **Figure 6. (Color online)** Pressure dependence of the interlayer Te_1-Te_1 and intralayer Bi-
518 Te_1, Bi-Te_2 and Sn-Te_2 distances of $SnBi_2Te_4$ (solid lines) and Bi_2Te_3 (dotted lines)
519 obtained from *ab initio* calculations.

520 **Figure 7.** Pressure dependence of the resistance of $SnBi_2Te_4$ recorded during loading
521 (filled symbols) and unloading (empty symbols).

522 **Figure 8. (Color online)** Calculated electronic band structure of $SnBi_2Te_4$ at 0, 3.9, 4.5
523 and 5.2 GPa. Reference energy (0 eV) has been taken as the maximum of the valence
524 band. A tentative position of the Fermi level in a highly-doped p-type sample is indicated
525 by the horizontal red dashed line.
526
527 **Figure 9. (Color online)** Calculated electronic band structure of Bi_2Te_3 at 0, 3.3, 4.1 and
528 5.0 GPa. Reference energy (0 eV) has been taken as the maximum of the valence band.
529 A tentative position of the Fermi level in a highly-doped p-type sample is indicated by
530 the horizontal red dashed line.

531 **Figure 1a**

532

533

534

535

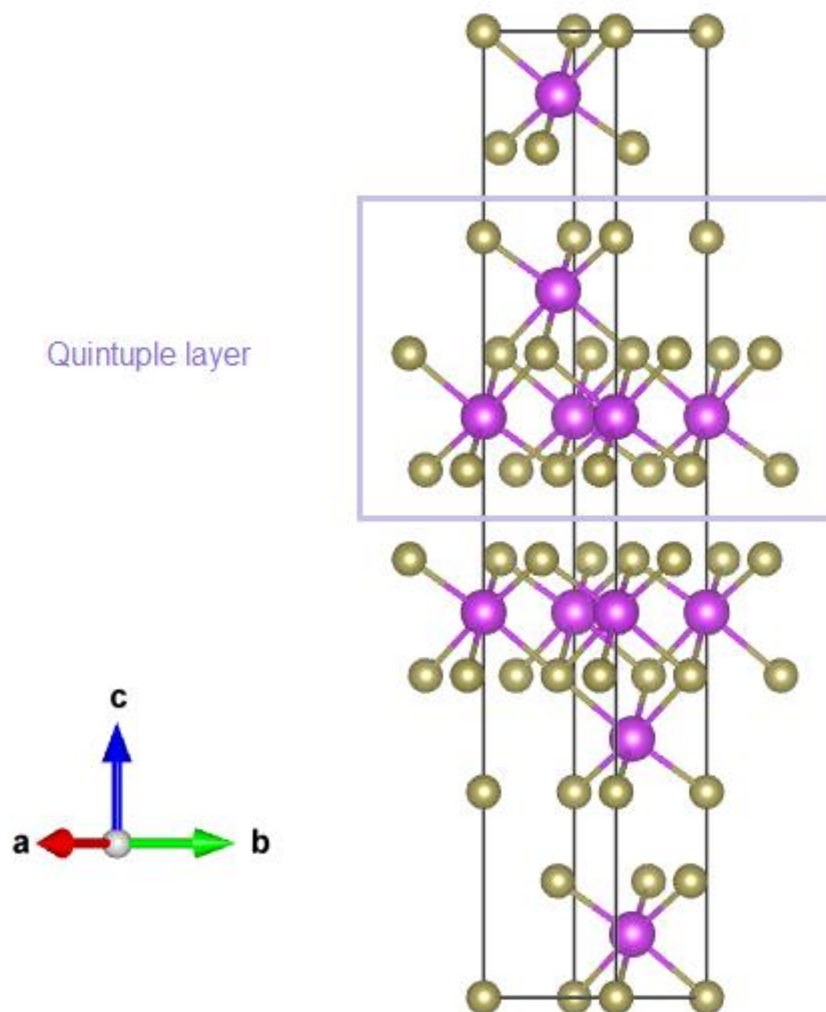

536

537

538

539

540

541

542

543

544

545

546

547

548

549

550 **Figure 1b**

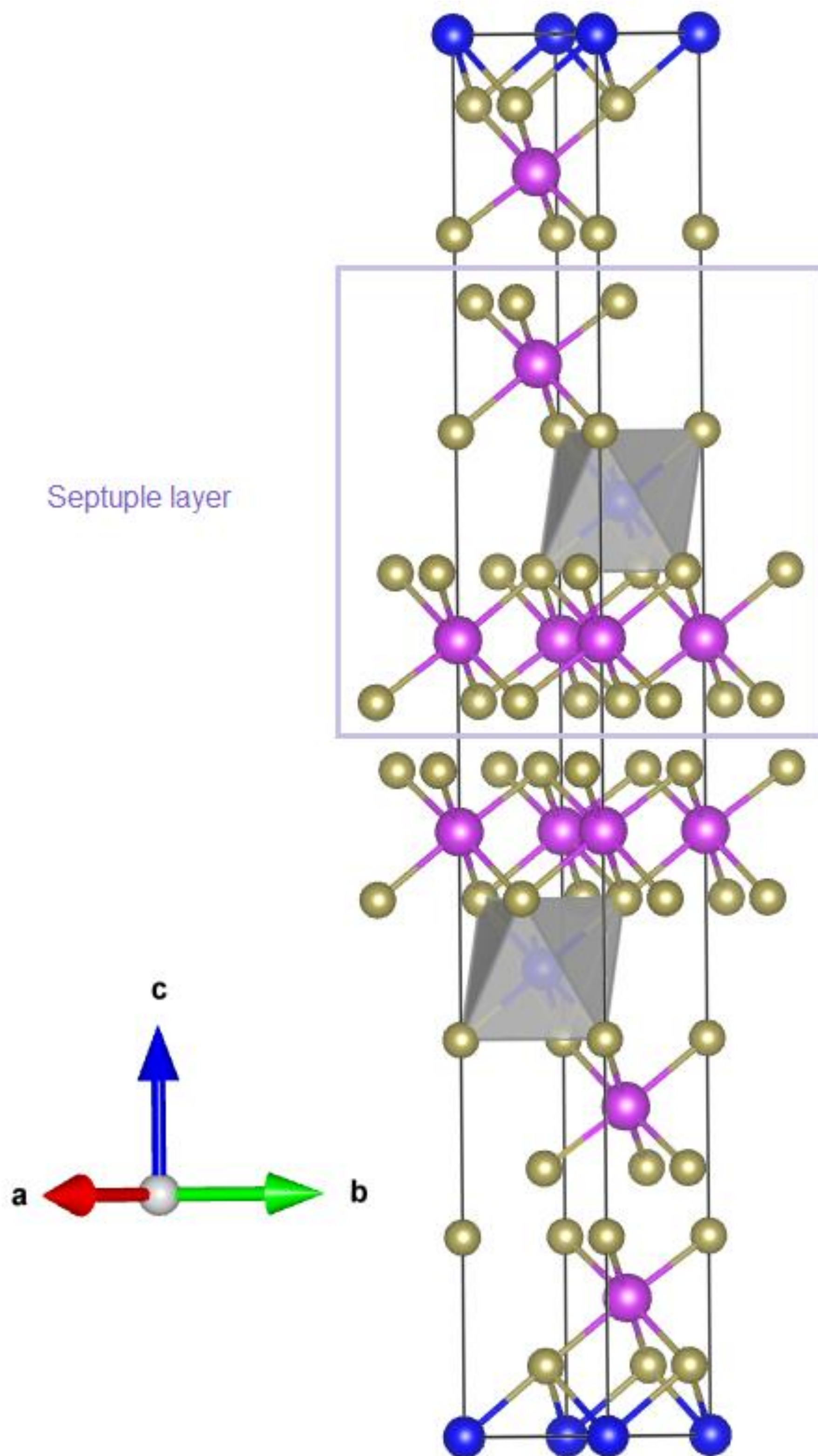

551
552
553
554
555

556 **Figure 2**

557

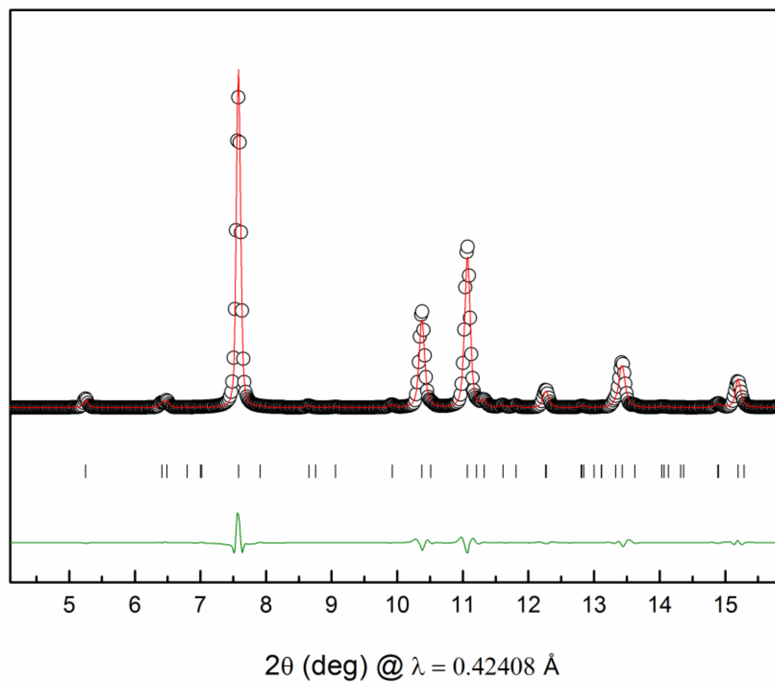

558
559
560
561
562
563
564
565
566
567
568
569
570
571
572
573
574
575
576
577
578
579

580 **Figure 3**

581

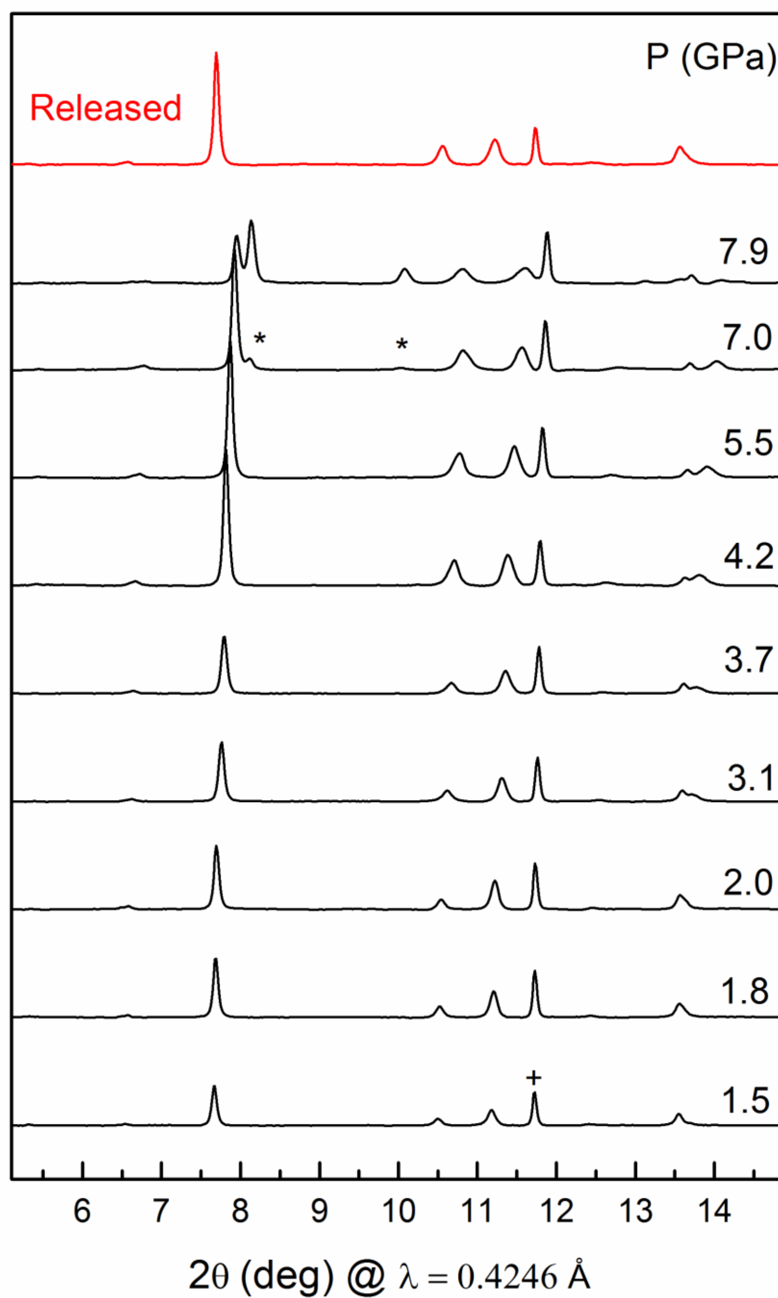

582

583

584 **Figure 4**

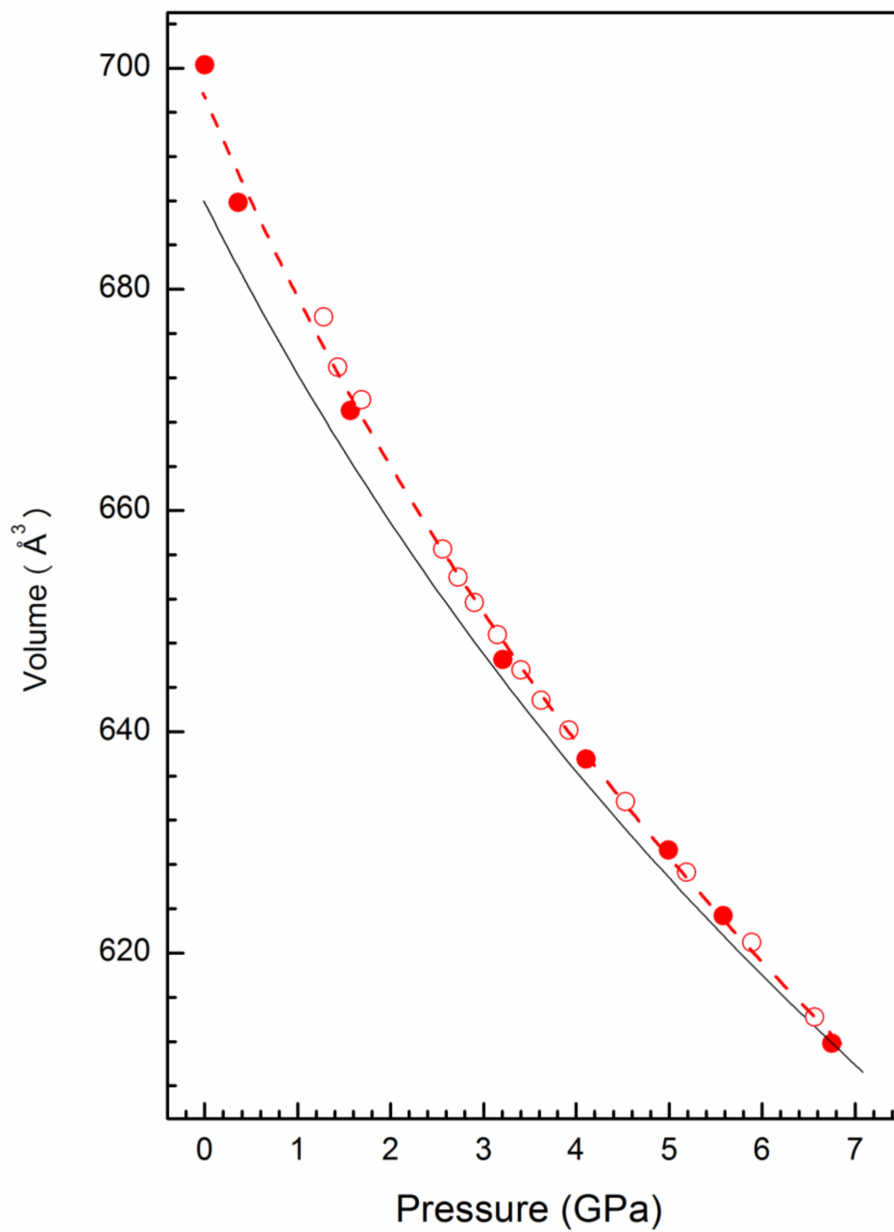

585

586

587

588

589 **Figure 5**

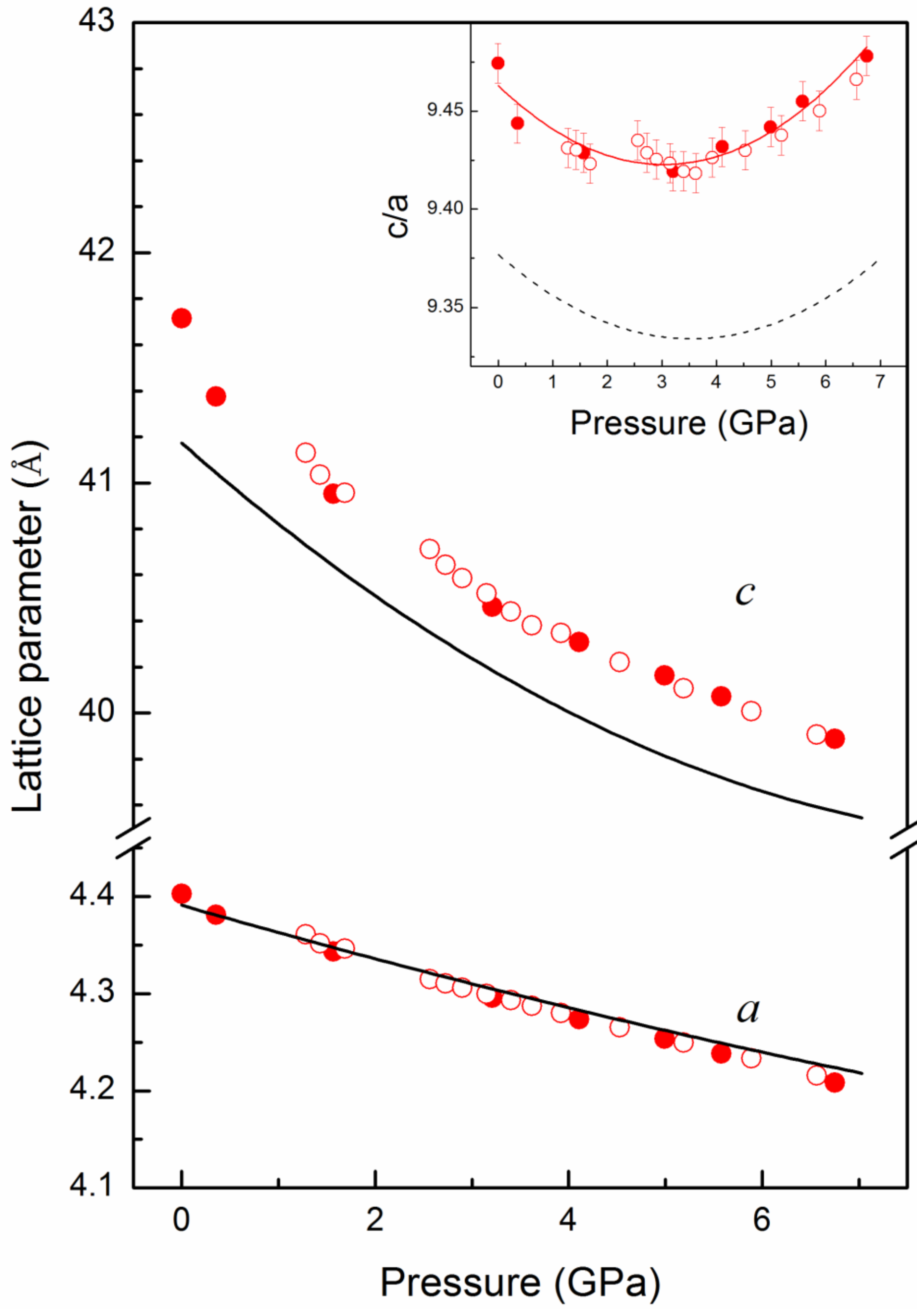

590

591
592
593 **Figure 6**
594

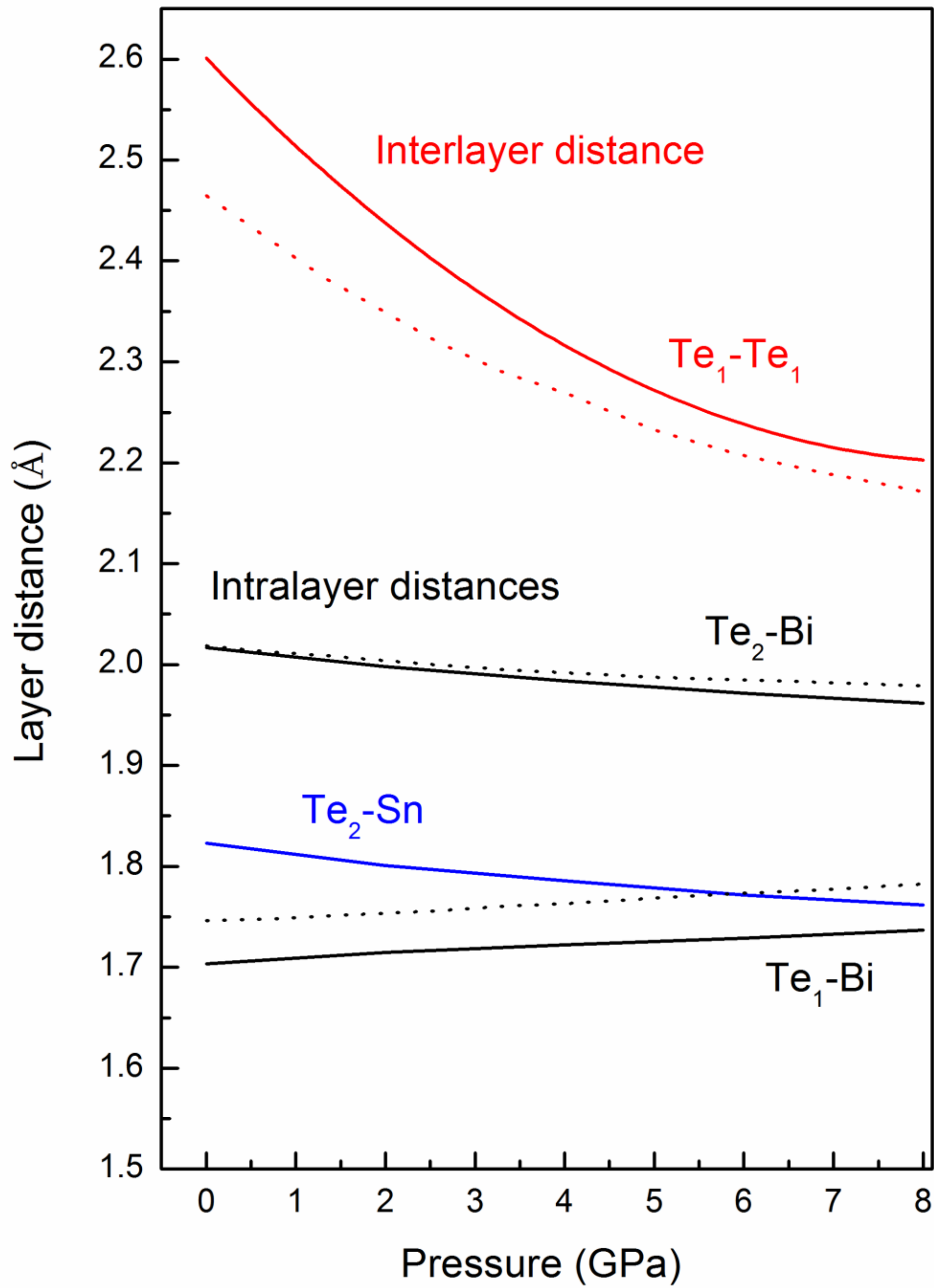

595

596
597 **Figure 7**
598
599

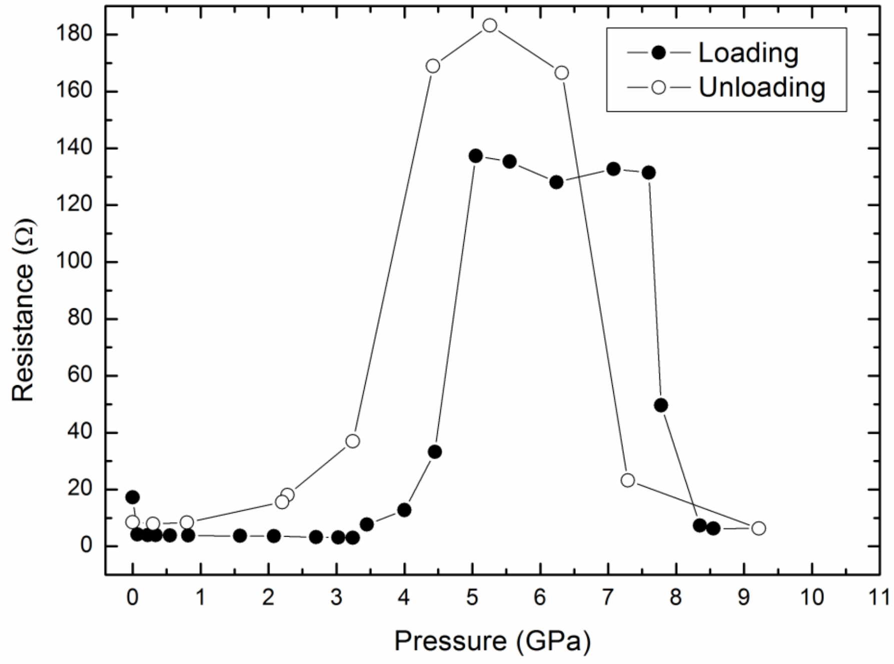

Figure 8

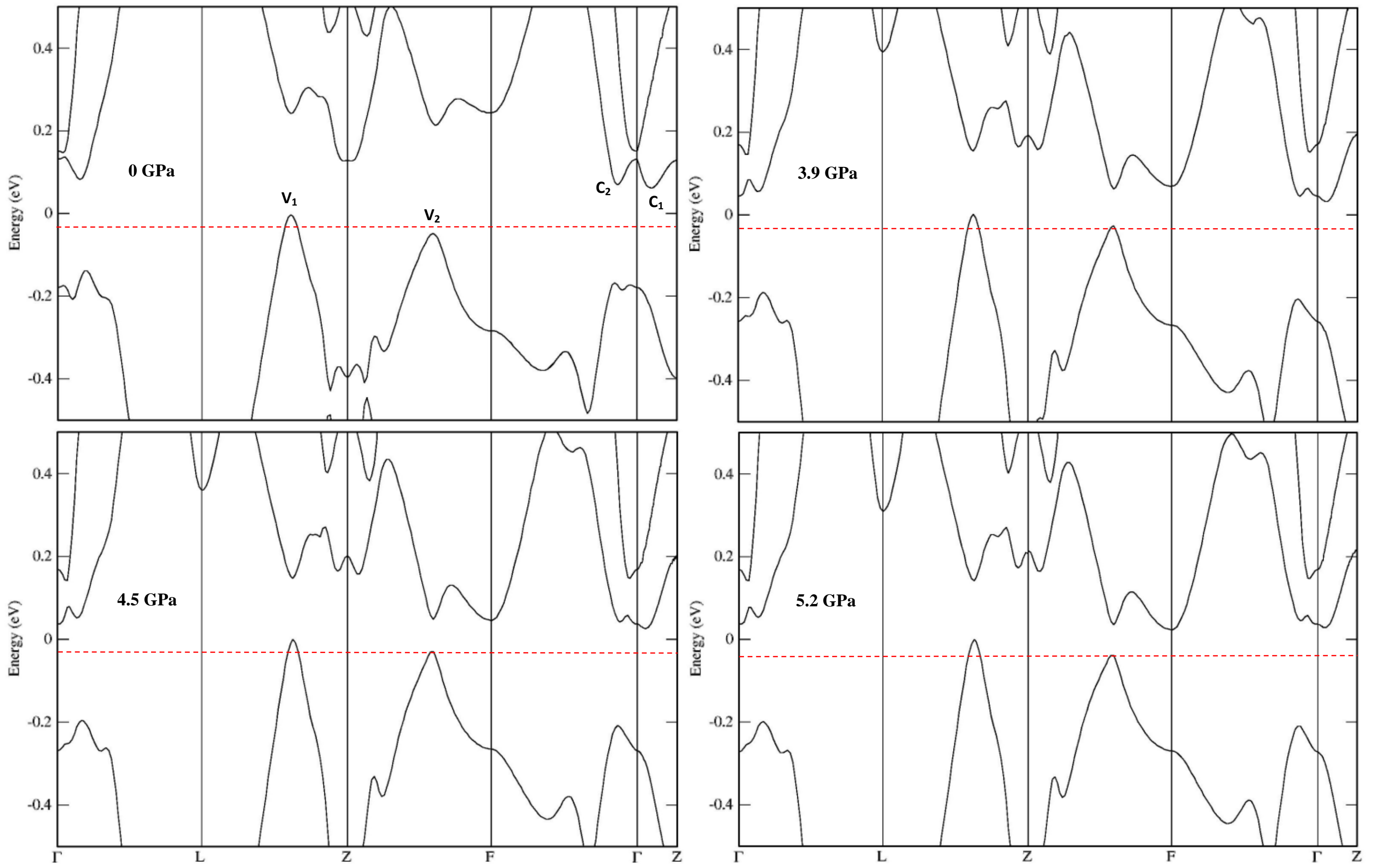

Figure 9